

## Article

# Study of Copper/Aluminum Bimetallic Tube Rotary Ring Spinning Composite Forming Characteristics

Chen Wang , Binkai Zhang, Dongfang Yao, Zhuangzhuang Tian and Chunjiang Zhao

School of Mechanical Engineering, Taiyuan University of Science and Technology, Taiyuan 030024, China

\* Correspondence: wangc1215@163.com

**Abstract:** As a plastic forming process developed based on rotary wheel spinning technology, the rotary ring spinning process has the excellent characteristics of high forming accuracy and high material utilization rate, and has been gradually applied to the manufacture of bimetallic composite pipes. In this paper, the forming law of a bimetallic tube in the process of rotary ring spinning was analyzed by numerical simulation and experimentation. The results show that the deformation coordination of the basic and cover tubes increased with the increasing press amount, and the feed ratio had less of an effect on the thickness variation. In addition, the three-way strain of the basic and cover tubes and the degree of influence of the process parameters on the equivalent strain of the tubes were also studied. The results show that the radial strain on both tubes was the largest, followed by the axial strain, and the tangential strain was the smallest; the press amount had the largest effect on the equivalent strain of the tubes, followed by the angle of attack and the feed ratio. These results provide some guidance for the manufacture of high-performance bimetallic composite tubes by rotary ring spinning.

**Keywords:** bimetallic composite tube; rotary ring spinning; three-way strain; deformation characteristic



**Citation:** Wang, C.; Zhang, B.; Yao, D.; Tian, Z.; Zhao, C. Study of Copper/Aluminum Bimetallic Tube Rotary Ring Spinning Composite Forming Characteristics. *Appl. Sci.* **2023**, *13*, 4727. <https://doi.org/10.3390/app13084727>

Academic Editor: Alberto Campagnolo

Received: 19 February 2023

Revised: 5 April 2023

Accepted: 7 April 2023

Published: 9 April 2023



**Copyright:** © 2023 by the authors. Licensee MDPI, Basel, Switzerland. This article is an open access article distributed under the terms and conditions of the Creative Commons Attribution (CC BY) license (<https://creativecommons.org/licenses/by/4.0/>).

## 1. Introduction

A bimetallic composite tube combines two metals through various deformation and connection technologies to make the tube layers tightly connected. When subjected to certain external forces, the basic tube and cover tube can be deformed simultaneously without separation at the bonding interface. A bimetallic composite tube has the characteristics of the basic tube and cover tube at the same time, giving full play to the performance of both tubes; this includes not only great intensity and stiffness, but also superior anticorrosion ability, light weight, high mechanical strength, and other properties [1]. At present, bimetallic composite tubes are extensively used in electrical power, space aviation, air-conditioning ducts, military engineering, and other applications.

Plastic processing technology is an important class of manufacturing for forming bimetallic composite materials, which mainly includes hydraulic expansion [2], tube sinking [3], explosion welding [4], tube extrusion shearing [5], magnetic pulse cladding [6], rotary wheel spinning [7], and other processes. Among them, rotary wheel spinning forming technology has the advantages of excellent performance, high material utilization, and process flexibility [8]. As a new kind of technology for forming composite tubes developed based on rotary wheel spinning, rotary ring spinning has the benefits of a simple process, high deformation efficiency, and low investment.

For the past few years, many scholars have undertaken related studies and work on rotary wheel spinning technology. Jin et al. [9] investigated the hardness variation and three-way strain of basic and cover tubes after rotary wheel spinning by numerical simulation and experimental methods. Guo et al. [10] used the theoretical knowledge of elasto-plastic mechanics to study the stress-strain dynamics of internal rotating wheels during the spin-forming process, and proposed a theoretical model of the elasto-plastic

boundary position, which was finally verified by simulation and testing. Qiwei et al. [11] used finite element simulation and experiments to investigate the stresses and thickness variations of bimetallic composite tubes of two materials, copper and aluminum, during the rotary wheel spinning composite process. Zhang et al. [12] investigated the influence of technological parameters such as thickness thinning, process temperature, feed rate, and post-annealing temperature on the combined strength of steel/aluminum bimetallic tubes in the rotary wheel spinning composite forming process. Xu et al. [13] used numerical simulations, an orthogonal experimental design, and polar differences to obtain significant process parameters for the rotary wheel spinning of bimetallic composite tubes, and verified the accuracy of the process parameters by experimentation. Yu et al. [1] carried out research on the stress, strain, and shear bond strength of copper/aluminum bimetallic composite tubes during rotary wheel spinning and forming through simulation, and investigated the impact law of the main technological parameters on the shear bond strength of bimetallic tubes through experiments and simulations. Xu et al. [14] investigated the effects of the original thickness ratio, heat treatment temperature, and thinning amount on the spinning bond strength and deformation synchronization of aluminum/aluminum composite tubes by process tests and finite element simulations.

While many scholars have carried out enriching studies on rotary wheel spinning, little research has been reported on the forming process of rotary ring spinning. Rotary ring spinning technology inherited the advantages of a simple process, low cost, and high forming efficiency. However, the relationship between the basic tube and the cover tube in the forming process of rotary ring rolling directly affects the molding quality and wall thickness distribution of bimetallic composite tubes, and plays a determinative role in the adjustment of the process parameters. In this study we used a method that integrates numerical simulation and experimentation to investigate the stresses during the rotary ring spinning forming process and the effects of different technological parameters on the thickness and three-way strain of bimetallic tubes. We also investigated the extent of the impact of the main technological parameters on the equivalent strain of the basic tube and the cover tube. The precision of the simulation model was validated by comparing the experimental and simulation results.

## 2. Materials and Methods

The rotary ring spinning forming process is similar to the spin wheel spinning forming process. The principle is that the rotary ring rotates at high speed around the axis of the spindle, while the tube is fed axially through the rotary ring, and depending on the shape and size of the rotary ring, the bimetallic composite tube will have coordinated plastic deformation. The contact between the bimetallic tube and the spinning ring generates a large amount of frictional heat, which will affect the rollable performance of the bimetallic tube and the service life of the rotary ring. In order to eliminate this phenomenon, during the forming process, the spinning ring is free to rotate around its central axis under the action of friction, and its direction of rotation is opposite to the direction of spindle rotation. The principle of rotary ring spinning and the spinning equipment are shown in Figure 1. The experimental equipment is capable of reaching infinitely variable speeds of up to 330 r/min for the rotation of the rotary ring, and the feed rate can be adjusted between 0.8 and 8 mm/s.

The experimental materials used were H65 brass and 6063 aluminum alloy, and the chemical composition of the two materials is given in Tables 1 and 2, respectively [15,16]. The mechanical properties at room temperature are shown in Table 3 [17–21]. H65 was used for the cover tube with an inner dimension of 53 mm, and the 6063 aluminum alloy was used for the basic tube with an inner dimension of 51 mm. Both tubes had a wall thickness of 1 mm and length of 35 mm. To eliminate the oxide coating and obtain a clean bonded surface before the spinning process, the surface to be combined was skimmed in acetone and scrubbed with a stainless column brush [10].

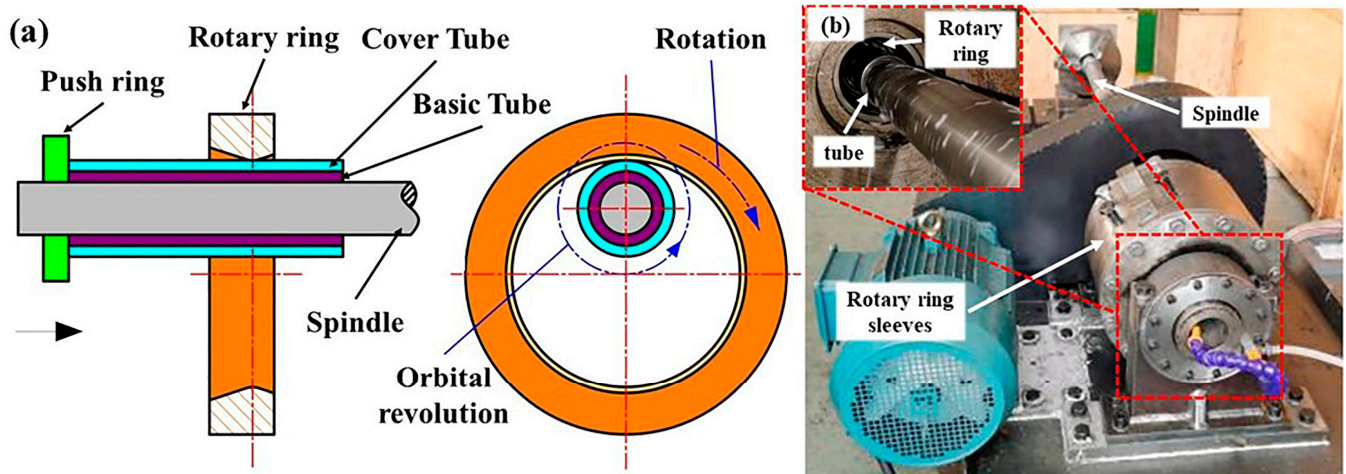


**Figure 1.** Schematic of the rotary ring spinning forming process and experimental equipment: (a) Schematic; (b) equipment.

**Table 1.** Chemical composition of H65 (weight fraction (%)).

Cu	Fe	Pb	Sb	Zn
64.50	0.035	<0.001	<0.001	35.40

**Table 2.** Chemical composition of 6063 (weight fraction (%)).

Mg	Si	Fe	Cu	Mn	Zn	Cr	Ti	Al
0.603	0.462	0.173	0.016	0.018	0.005	0.006	0.053	Bal

**Table 3.** Main mechanical characteristics of materials at room temperature.

	Density (Kg/m <sup>3</sup> )	Young's Modulus (GPa)	Poisson Ratio	Yield Stress (MPa)	Tensile Strength (MPa)	Elongation (%)
6063	2700	68.9	0.33	172	216.6	13.5
H65	8525.4	105	0.33	205	431.5	28.3

### 3. Finite Element Model for Rotary Ring Spinning

Based on large commercial ABAQUS/Explicit applications, the finite element model of bimetallic composite tube rotary ring spinning was established, as shown in Figure 2. The fixed spindle applies a thrust load to the side of the composite tube to make an axial feeding motion, while the rotary ring makes an eccentric revolution around the axis of the tube to achieve the forming process. The spindle and rotary ring are defined as rigid parts, the basic tube and cover tube are defined as deformation parts, the C3D8R solid cell is used to divide the mesh, and the thickness direction is set to a three-layer mesh to guarantee precise computation. The analysis step uses an explicit dynamic model, using the Coulomb friction condition to define the contact, with the friction factor between the rotary ring and the tube set to 0.3, the inside surface of the cover tube and the outside surface of the basic tube to 0.2, and the tube and spindle to 0.1 [11]. All contact surfaces are set to “face-to-face contact” to allow relative sliding between them. In the finite element simulation, the composite tube is stripped of parts that are not involved in the deformation in order to decrease the computational time. Otherwise, all geometric dimensions and loading conditions of the finite element model are identical to the experimental procedure.

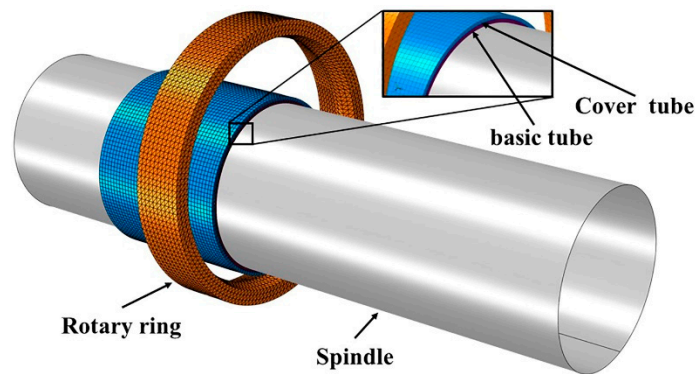


Figure 2. Finite element model of bimetallic tube rotary ring spinning.

#### 4. Results and Discussion

##### 4.1. Analysis of the Force in the Process of Rotary Ring Spinning

Because of the wide discrepancy in the mechanical characteristics of the basic and cover tube materials, the deformation of the metal in the spinning area during the rotary ring spinning process is complex, which results in different forces on the basic and cover tubes. In addition, the presence of friction between the two tubes causes a different stress distribution in their spinning area directly below the downward pressure of the rotary ring. Figure 3 shows the distribution of the equivalent stress in the rotary ring spinning process of a bimetallic tube.

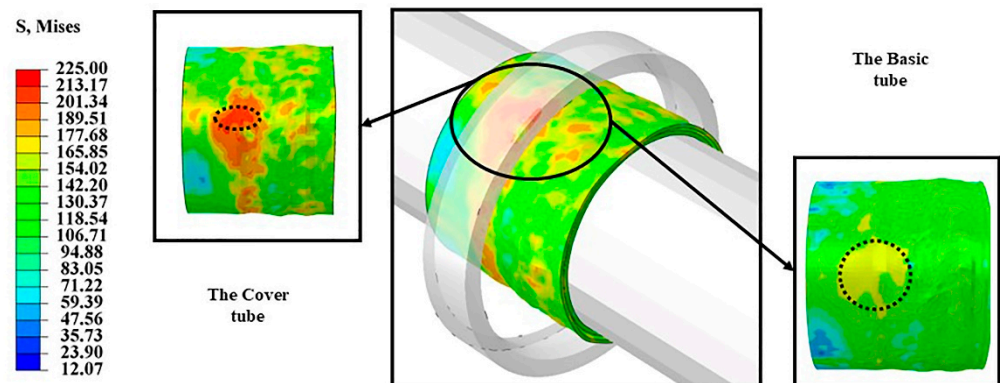
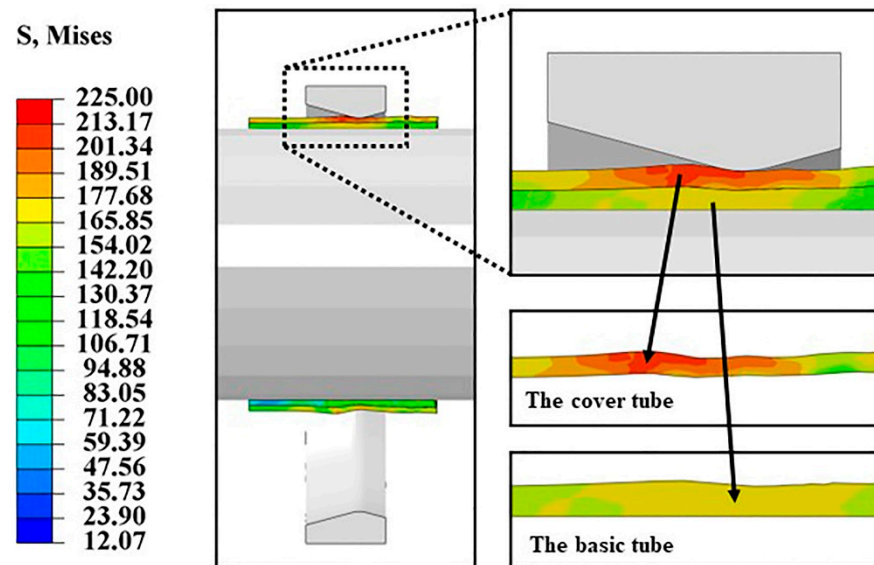


Figure 3. Equivalent stress distribution during rotary ring spinning of bimetallic tube.

From Figure 3, it can be seen that, in terms of magnitude, high stresses are generated in the downward pressure area of the rotating ring, and the difference in the largest equivalent stress of the basic tube and the cover tube is large; in terms of area, the largest equivalent stress between the basic tube is greater in the stress area. In the rotary ring spinning process, the cover tube only contacts the rolled part of the rotary ring and the contact area is limited, while the outside surface of the basic tube contacts the inside surface of the cover tube and the contact area is larger; thus, the area of maximum equivalent stress generated by the basic tube is also larger.

Figure 4 shows the distribution of radial equivalent stress during the rotary ring spinning of a bimetallic tube. It can be seen that in terms of stress magnitude and stress area, both show a similar pattern to the distribution of equivalent stress, with the basic tube being subjected to dispersed stress and the cover tube being subjected to concentrated stress; there is less variation in the distribution in the radial direction, as the size of the tubes is only 1 mm in the radial direction.



**Figure 4.** Distribution of radial equivalent stress during the rotary ring spinning of a bimetallic tube.

During the forming process, the boundary between the two tubes has a material discontinuity, and a pair of forces is applied to the outer surface of the basic tube and the inner surface of the cover tube, which results in different stresses on the tubes due to the different areas of forces on them. Therefore, the cover tube is subjected to much greater stress than the basic tube, as shown in Figures 3 and 4. In order to make the distortion of the two tubes more coordinated during the rotary ring spinning, the yield strength of the basic tube should be lower than that of the cover tube, otherwise the basic tube may not enter the plastic deformation stage during the plastic deformation of the cover tube, which would lead to uncoordinated deformation of both tubes, and then to the inability to form an effective interface strength.

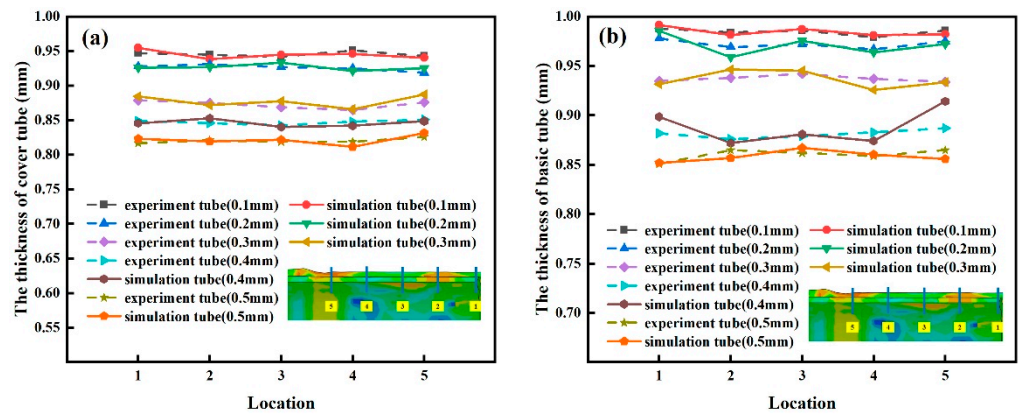
#### 4.2. Study of Rotary Ring Spinning Process Parameters

Since different material characteristics, tube dimensions, and process parameters have different effects on the thickness variation and three-way strain during the rotary ring spinning process, we focused on the influence of the main process parameters (press amount, feed ratio, and angle of attack) on the thickness variation and three-way strain of the basic cover tube during the rotary ring spinning process.

##### 4.2.1. Press Amount

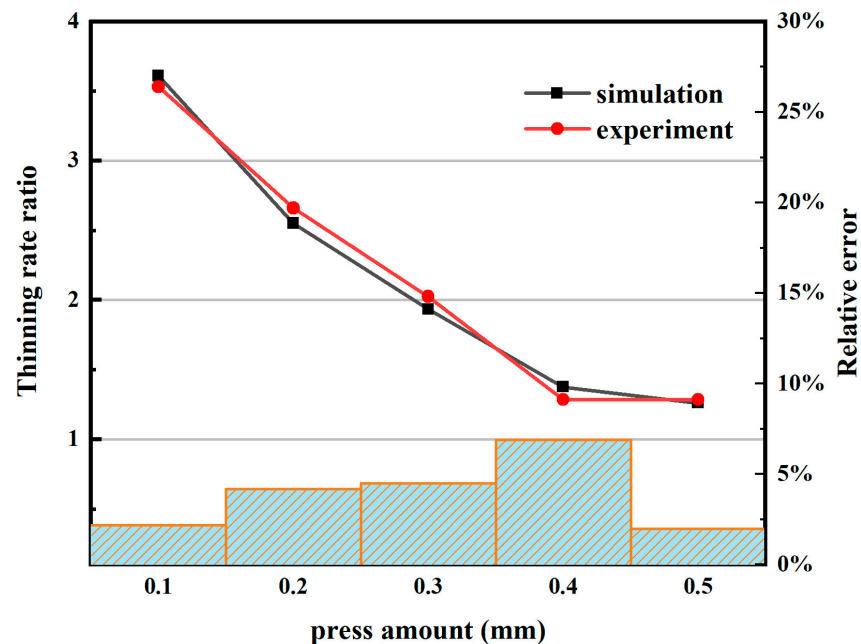
In the process of bimetallic tube rotary ring spinning, the press amount directly reflects the degree of thinning of the composite tube, so it has a large impact on the thickness variation of the bimetallic composite tube and the three-way strain distribution; therefore, in this paper we adopted the single-factor control method to analyze the influence law of the press amount on the forming quality. The press amount was taken as 0.1, 0.2, 0.3, 0.4, and 0.5 mm, and the other process parameters were kept unchanged, with a feed ratio of 0.4 mm/r and an angle of attack of the rotary ring of 18°.

Figure 5 shows the simulated and experimental results of thickness after rotary ring spinning with different press amounts. It can be seen that the corresponding thicknesses in the simulation and the experiment are basically the same. Considering the deformation of the rotary ring in the experiment, the non-uniform distribution of surface roughness, and other objective factors, there will be some deviation between the simulation and experiment, but it does not affect the accuracy of the model. The wall thickness of both the cover tube and the basic tube decreases as the press amount increases.



**Figure 5.** Simulated and experimental results of thickness after rotary ring spinning with different press amounts: (a) cover tube; (b) basic tube.

Figure 6 shows the ratio of the thinning rate of the cover and basic tubes after rotary ring spinning with different press amounts; it can be seen that the ratio trends toward 1 as the press amount increases. Since the wall thickness of both tubes is the same, it is known from the principle of volume invariance that when the ratio of the thinning rate of the tubes is closer to 1, the harmonization of the distortion between the two will be better. Therefore, an increased press amount will promote the coordination of the deformation of the basic cover tube somewhat. As can be seen in Figure 6, the experimental data are within 8% error of the simulated data for the range of process parameters studied, thus verifying the accuracy of the model.



**Figure 6.** Ratio of thinning rate of cover and basic tubes after rotary ring spinning.

Figure 7 shows the simulated distribution of equivalent strain after rotary ring spinning with different press amounts. It can be seen that with an increased press amount, the equivalent strain of the bimetallic tube also increases, the difference in axial deformation between the basic and cover tube gradually decreases, and the deformation becomes more coordinated.

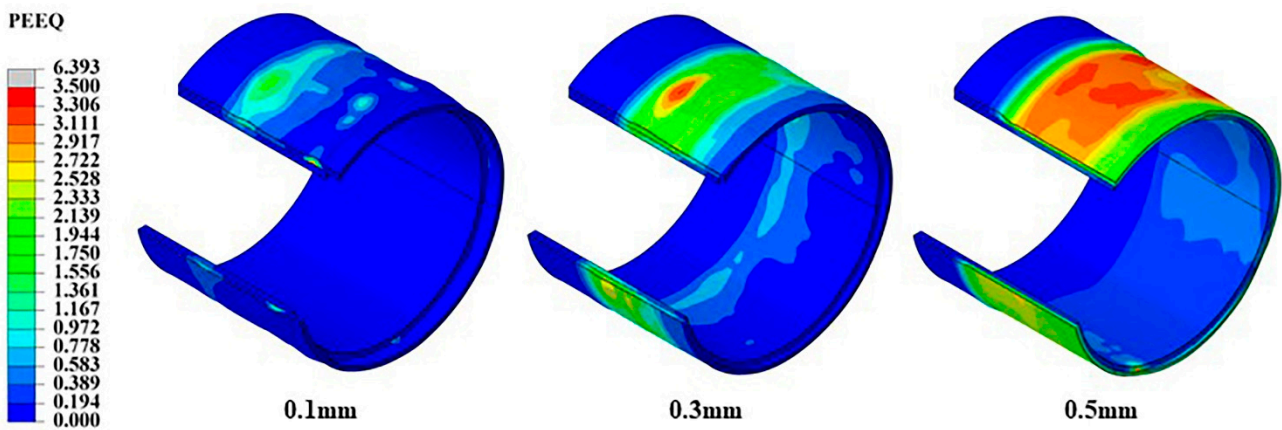


Figure 7. Simulated distribution of equivalent strain after rotary ring spinning with different press amounts.

Figure 8 shows the three-way strain distribution for the basic tube and cover tube with different press amounts. As can be seen in the Figure 8, the three-way strain is greater on the cover tube than the basic tube, and increases as the press amount increases. The strain distribution in the radial, axial, and tangential directions shows that the radial strain is the largest, followed by the axial, and the tangential is the smallest. This is because as the rotary ring spinning process proceeds, the metal buildup will have a detrimental effect on the axial flow of the metal, and the axial strain of the basic cover tube will be reduced compared to the radial strain, ultimately resulting in an increasing difference between the two.

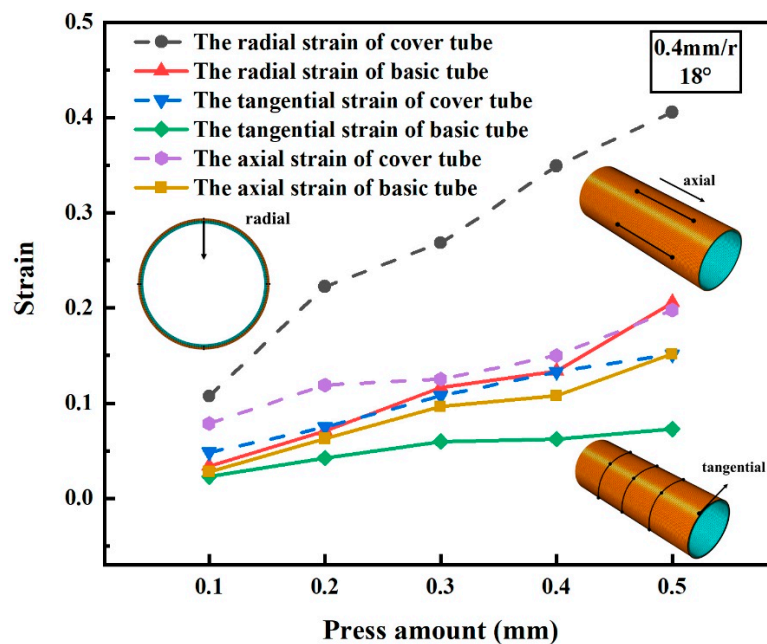


Figure 8. Three-way strain distribution for basic and cover tubes with different press amounts.

#### 4.2.2. Feed Ratio

The feed ratio is the ratio of the axial feed of the tube to the number of revolutions per unit of time during the rotary ring spinning. The single factor control method was used to analyze the influence of the feed ratio on the forming quality. The feed ratios were taken as 0.2, 0.3, 0.4, 0.5, and 0.6 mm/r, while other process parameters remained unchanged, with a press amount of 0.3 mm and an angle of attack of the rotary ring of 18°.

Figure 9 shows the variation in average thickness and the ratio of thinning rate after rotary ring spinning with different feed ratios. It can be found that the average wall thickness of the basic and cover tubes is basically the same under different feed ratios, and

there is a small difference in the ratio of the thinning rate between the two tubes, so the feed ratio has little effect on the thickness of the bimetallic tube. The reduced feed ratio increases the rotary ring revolution speed at the same feed rate, and the contact frequency between the tube and the rotary ring is more frequent, but the area of contact remains the same, so there is basically no significant difference in thickness.

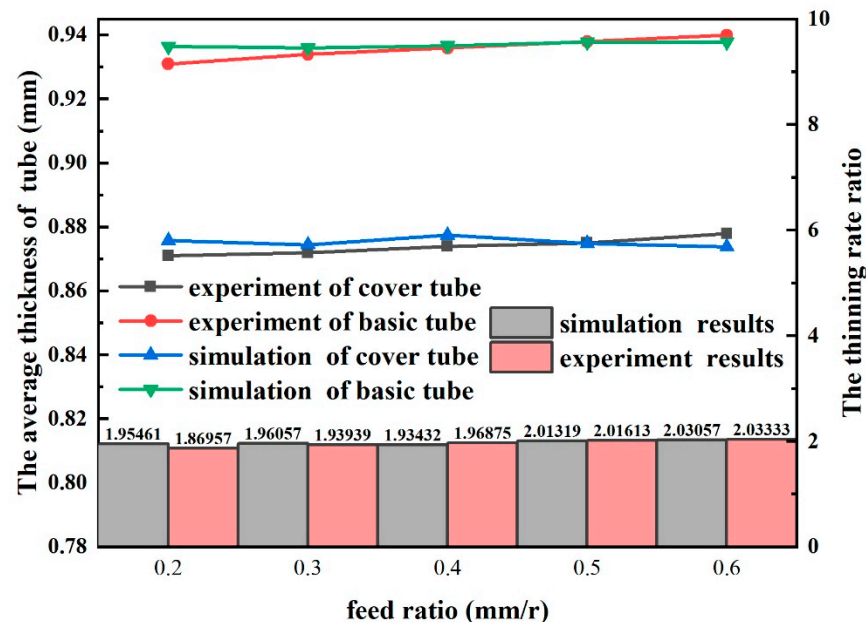


Figure 9. Variation of average thickness and ratio of thinning rate after rotary ring spinning with different feed ratios.

Figure 10 shows the distribution of the three-way strain of the basic and cover tubes after rotary ring spinning with different feed ratios. It can be seen from the figure that the axial and tangential strains of both tubes decrease accordingly as the feed ratio increases and the radial strain remains constant, and the rebound is less for lower feed ratios. The analysis shows that a lower feed ratio will make the rotary ring turn more through the contact deformation zone of the tube per unit time, with more frequent contact between the tube and the rotary ring per unit area, thus improving the material flow; this effectively reduces the amount of rebound in the intensive extrusion process.

#### 4.2.3. Angle of Attack of the Rotary Ring

The angle of attack of the rotary ring is the angle between the formed contact surface of the rotary ring and the tube and the axial direction of the spindle, as shown in Figure 11. The single factor control method was used to simulate the rotary ring spinning forming by taking  $12^\circ$ ,  $15^\circ$ ,  $18^\circ$ ,  $21^\circ$  and  $24^\circ$  as the angle of attack, and the other process parameters were kept unchanged, with a press amount of 0.3 and feed ratio of 0.4 mm/r.

Figure 12 shows the simulation results of thickness after rotary ring spinning with different angles of attack. It can be seen that as the angle of attack of the rotary ring decreases, the wall thickness of the basic tube becomes smaller, and the thickness of the cover tube becomes larger. As the angle of attack of the rotary ring decreases, the area of contact between the rotary ring and the cover tube increases, which leads to the convergence of forces on the basic and cover tubes. Furthermore, since copper is stronger than aluminum, along with the reduced angle of attack of the rotary ring, the thinning of the basic tube increases, the thickness is reduced, and the thinning of the cover tube decreases; thus, the wall thickness becomes larger.

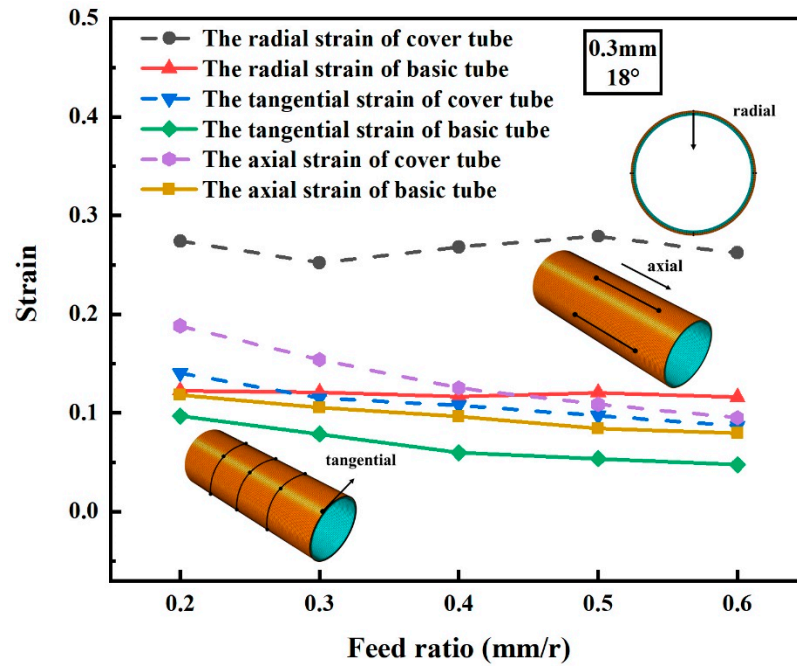


Figure 10. Three-way strain distribution for basic and cover tubes with different feed ratios.

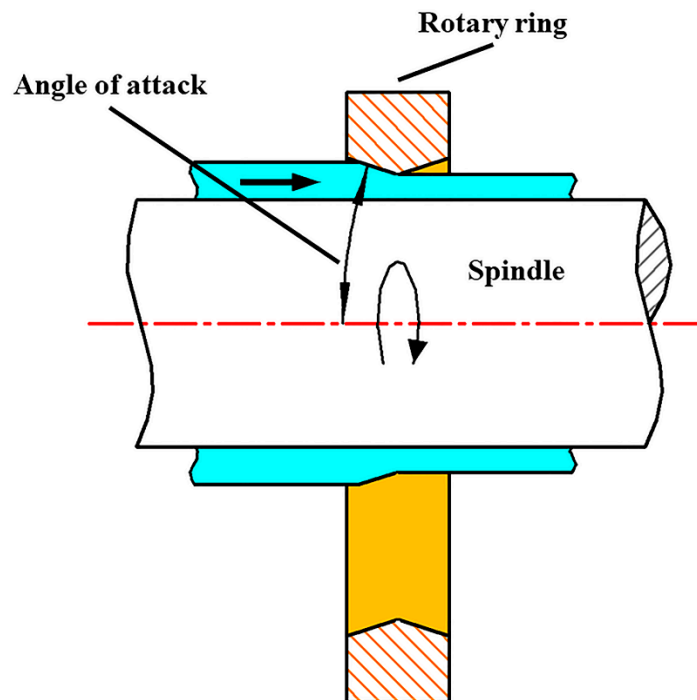


Figure 11. Diagram of angle of attack of rotary ring.

Figure 13 shows the distribution of three-way strain in the basic and cover tubes after rotary ring spinning at different angles of attack. It can be found that the radial strain of the two tubes is less affected by the angle of attack of the rotating ring, and with decreased angle of attack, axial and tangential strains increase by 12.45 and 27.84%, respectively, with the increase being larger for the cover tube than the basic tube. The analysis shows that as the angle of attack decreases, the area of contact between the rotary ring and the tube increases, and the volume of the tube involved in deformation increases at the same time; in turn, the axial and tangential strains of the tube will increase by a certain amount. In addition, during the spinning process, smaller angles of attack lead to an increase in the

applied load on the tube, which causes more metal to flow to the undeformed area, leading to an expansion of the actual thickness of the cover tube involved in spinning; this then leads to a greater increase in the equivalent strain of the cover tube than the basic tube.

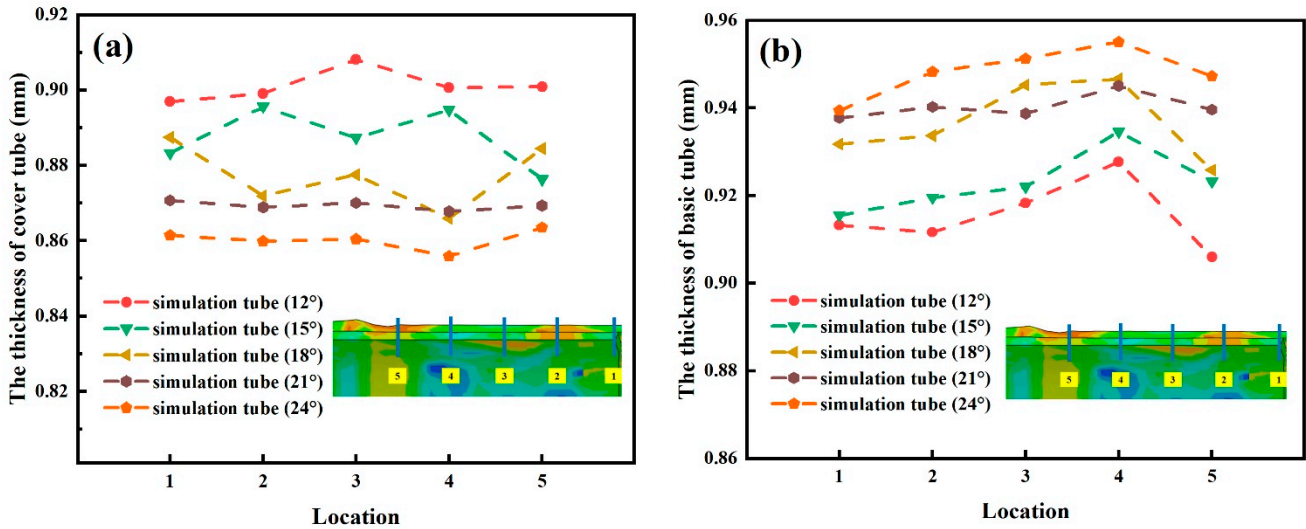


Figure 12. Simulated results of thickness after rotary ring spinning with different angles of attacks: (a) cover tube; (b) basic tube.

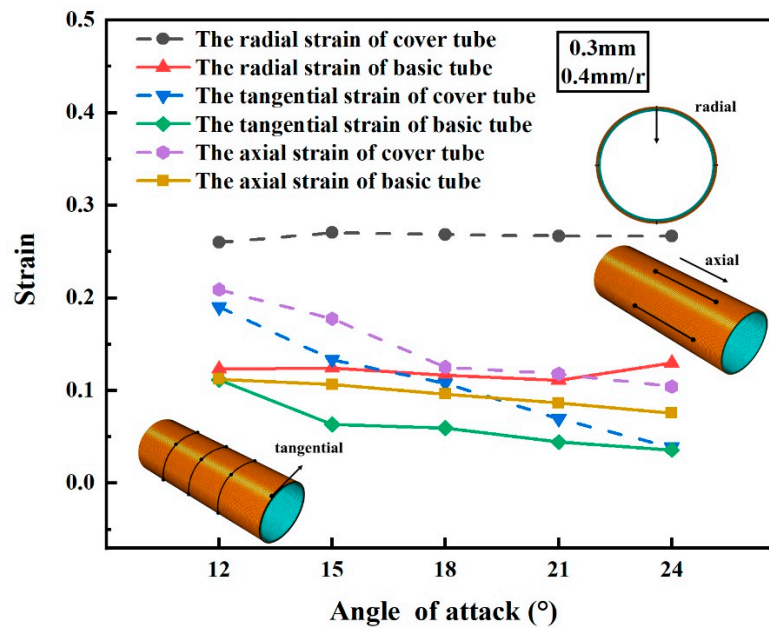


Figure 13. Three-way strain distribution for basic and cover tubes at different angles of attacks of rotary ring.

From the above, it can be seen that a smaller angle of attack helps the plastic deformation of the metal, but a too small angle of attack is not conducive to biting into the tube. The radial compressive strain and axial tensile strain contribute to the plastic flow of the metal material [22]; when the axial flow rate of the metal is less than the feeding speed of the tube, it will lead to a certain accumulation of metal in front of the axial feeding direction of the rotary ring, which will greatly reduce the forming quality of the composite tube.

### 4.3. The Effect of Rotating Ring Spinning Process Parameters on Equivalent Strain

It has been shown that sufficient plastic deformation helps to increase the bonding strength of the composite [23]. In order to further evaluate the effect of the rotary ring spinning process parameters on the equivalent strain, the equivalent strain sensitivity factor  $S$  is proposed. When the process parameters change, the difference between the equivalent strain under each process parameter and under the intermediate process parameters can be calculated. This difference is characterized by  $S$ , expressed by Equation (1):

$$S = \frac{\varepsilon_{PE} - \varepsilon_{PE}^0}{\varepsilon_{PE}^0} \times 100\% \tag{1}$$

where  $\varepsilon_{PE}$  is the equivalent strain for each process parameter and  $\varepsilon_{PE}^0$  is the equivalent strain for intermediate process parameters.

Combined with the above information, the intermediate process parameters are as follows: 0.3 mm press amount, 0.4 mm/r feed ratio, and 18° angle of attack. The range of study parameters for the rotary ring spinning process is given in Table 4.

**Table 4.** Range of study parameters for the rotary ring spinning process.

Parameters	1	2	Middle	3	4
Press amount (mm)	0.1	0.2	0.3	0.4	0.5
Feed ratio (mm/r)	0.2	0.3	0.4	0.5	0.6
Angle of attack (°)	12	15	18	21	24

Figure 14 shows the distribution of the equivalent strain sensitivity coefficient for the basic and cover tubes with different sets of process parameters. The comparative analysis of the three curves in Figure 14 shows that the equivalent strain sensitivity coefficient is positively correlated with the press amount, and negatively correlated with the feed ratio and the angle of attack of the rotary ring. It also shows that when the press amount increases, the equivalent strain of the basic and cover tubes also increases, and the increased feed ratio and angle of attack of the rotary ring leads to slightly decreased equivalent strains of the tubes, which is the same as the above results. From the degree of inclination of the three curves, it can be found that the factors influencing the equivalent strain on the basic and cover tubes are, in order of priority, press amount, angle of attack, and feed ratio.

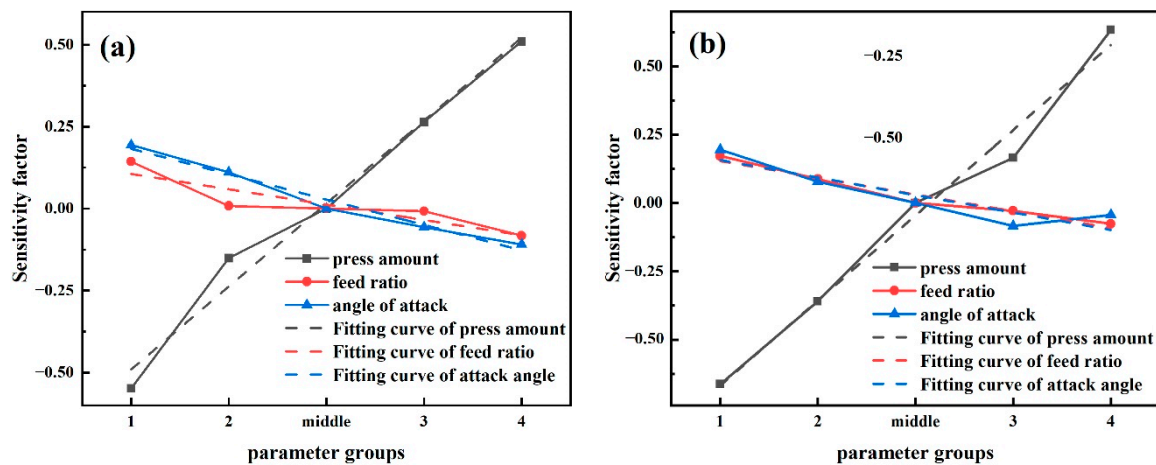


**Figure 14.** Distribution of the equivalent strain sensitivity coefficient for the basic and cover tubes with different sets of process parameters: (a) cover tube; (b) basic tube.

## 5. Conclusions

1. In order to make the distortion of the basic and cover tubes more harmonious, the yield strength of the basic tube should be less than that of the cover tube.
2. The three-directional strains of the basic and cover tubes are positively correlated with the press amount, with the radial strain being the largest, followed by the axial and tangential strains; the axial and tangential strains of the basic and cover tubes are negatively correlated with the feed ratio and the angle of attack.
3. Various process parameters affect the equivalent strain on the basic and cover tubes in the following order of priority: press amount, angle of attack, and feed ratio.

**Author Contributions:** Conceptualization, C.W.; methodology, C.W. and C.Z.; software, B.Z.; validation, D.Y. and Z.T.; formal analysis, C.W., C.Z. and B.Z.; investigation, C.W. and D.Y.; resources, C.W. and C.Z.; data curation, Z.T.; writing—original draft preparation, B.Z.; writing—review and editing, C.W.; visualization, D.Y.; supervision, C.Z.; project administration, C.W. and C.Z.; funding acquisition, C.W. All authors have read and agreed to the published version of the manuscript.

**Funding:** This research was funded by the Taiyuan University of Science and Technology Scientific Research Initial Funding (20202076), the Fundamental Research Program of Shanxi Province (20210302123275), and the Doctoral Starting Foundation of Shanxi Province (20212059).

**Institutional Review Board Statement:** Not applicable.

**Informed Consent Statement:** Not applicable.

**Data Availability Statement:** All relevant data are available in the article.

**Conflicts of Interest:** The authors declare no conflict of interest.

## References

1. Yuan, Q.W.; Wang, J.H.; Jin, K.; Tao, J. Finite Element Numerical Simulation and Analysis of Incremental Forming of Al/Cu Double Metal Tube Inner Spinning. *J. Netshape Form. Eng.* **2018**, *10*, 41–47.
2. Dong, J.S.; Ozturk, F.; Nieto, A.; Guo, T.Y.; Jarrar, F.; Sheikahmad, J.Y. Analysis of Process Parameters for Different Material Pairs of Mechanically Lined CRA Pipes Manufactured by Thermal-Hydraulic Expansion Process. *Teh. Vjesn.* **2021**, *28*, 1442–1447.
3. Halaczek, D. Analysis of Manufacturing Bimetallic Tubes by the Cold Drawing Process. *Arch. Metall. Mater.* **2016**, *61*, 241–248. [[CrossRef](#)]
4. Zhang, E.M.; Zhao, Y.M.; Wang, Z.M.; Li, W.Y. Effect of heat treatment on the microstructure and mechanical properties of structural steel-mild steel composite plates fabricated by explosion welding. *Int. J. Min. Met. Mater.* **2020**, *27*, 1115–1122. [[CrossRef](#)]
5. Tian, Y.; Hu, H.J.; Zhang, D.F. A novel severe plastic deformation method for manufacturing Al/Mg bimetallic tube. *Int. J. Adv. Manuf. Tech.* **2021**, *116*, 2569–2575. [[CrossRef](#)]
6. Fan, Z.S.; Yu, H.P.; Meng, F.C.; Li, C.F. Experimental investigation on fabrication of Al/Fe bi-metal tubes by the magnetic pulse cladding process. *Int. J. Adv. Manuf. Tech.* **2016**, *83*, 1409–1418. [[CrossRef](#)]
7. Ou, X.B.; Zhu, X.Y.; Gu, P.; Wang, B.C.; Li, J.; Liu, X.; Liu, C.; He, F.; Li, Q. Finite Element Analysis and Investigation on Spinning of Quadrilateral Parts with Hollow Cross-Sections Based on Hypocycloid Theory. *Appl. Sci.* **2020**, *10*, 8588. [[CrossRef](#)]
8. Liu, Y.L.; Shu, X.D.; Cen, Z.W.; Li, Z.X.; Ye, B.H. Effects of Process Parameters on Surface Straightness of Variable-Section Conical Parts during Hot Power Spinning. *Appl. Sci.* **2021**, *11*, 8187. [[CrossRef](#)]
9. Jin, K.; Yuan, Q.W.; Tao, J.; Domblesky, J.; Guo, X.Z. Analysis of the forming characteristics for Cu/Al bimetal tubes produced by the spinning process. *Int. J. Adv. Manuf. Tech.* **2019**, *201*, 147–155. [[CrossRef](#)]
10. Guo, X.Z.; Yu, Y.H.; Tao, J.; Wang, H.; El-Aty, A.A.; Wang, C.; Luo, X.Y.; Kim, N. Maximum residual contact stress in spinning process of SS304/20 bimetallic pipe. *Int. J. Adv. Manuf. Tech.* **2020**, *106*, 2971–2982. [[CrossRef](#)]
11. Yuan, Q.W.; Wang, J.H.; Jin, K.; Tao, J. Forming Characteristics of Cu/Al Bimetal Tube Spinning. *J. Netshape Form. Eng.* **2018**, *10*, 48–54.
12. Zhang, Z.P.; Xu, W.C.; Gu, T.S.; Shan, D.B. Fabrication of steel/aluminum clad tube by spin bonding and annealing treatment. *Int. J. Adv. Manuf. Tech.* **2017**, *94*, 3605–3617. [[CrossRef](#)]
13. Xu, W.B.; Yang, Y.Y.; Dai, C.W.; Xie, J.G. Optimization of spinning parameters of 20/316L bimetal composite tube based on orthogonal test. *Sci. Eng. Compos. Mater.* **2020**, *27*, 272–279. [[CrossRef](#)]
14. Xu, W.C.; Zhang, Z.P.; Huang, K.; Shan, D.B. Effect of heat treatment and initial thickness ratio on spin bonding of 3A21/5A03 composite tube. *J. Mater. Process Technol.* **2017**, *247*, 143–157. [[CrossRef](#)]
15. Xie, L.; Li, J.Y.; Gong, D.Y.; Xu, J.Z. Effects of different processes on microstructure and mechanical properties of H65 brass. *Mater. Sci. Technol.* **2020**, *36*, 1997–2009. [[CrossRef](#)]

16. Peng, C.Y.; Zhu, D.D.; Li, K.F.; Du, X.; Zhao, F.; Wan, M.P. Research on a Low Melting Point Al-Si-Cu (Ni) Filler Metal for 6063 Aluminum Alloy Brazing. *Appl. Sci.* **2021**, *11*, 4296. [[CrossRef](#)]
17. Tian, F.S.; Liu, J.W.; Zhang, W.X.; Zhao, X.N. Effect of annealing treatment on properties of H65 brass tube under liquid impact forming. *J. Plast. Eng.* **2022**, *29*, 66–73.
18. Wang, Q.T.; Wang, X.N.; Chen, X.M.; Huan, P.C.; Dong, Q.P. Interactive effects of porosity and microstructure on strength of 6063 aluminum alloy CMT MIX + Synchropulse welded joint. *Trans. Nonferrous Met. Soc. China* **2022**, *32*, 801–811. [[CrossRef](#)]
19. Yan, M.; Wang, Y.Y.; Dong, Y.H. Study on mechanical properties change of 6063-T6 aluminum alloy after being vacuum brazed. *China Foundry Mach. Technol.* **2020**, *55*, 25–28.
20. Hu, F.T.; Wang, F.X.; Zhang, Y.F. Z In-plane stress distribution and improvement strategy of U-shaped ribbing of backward extrusion 6063 aluminum alloy. *J. Plast. Eng.* **2021**, *28*, 98–102.
21. Jiang, H.B.; Yao, X.J.; Li, B.; Li, C.H. Numerical simulation on deformation process for h65 brass based on continuous extrusion. *Hot Work. Technol.* **2010**, *39*, 21–23, 28.
22. Jiang, S.Y.; Zhang, Y.Q.; Zhao, Y.N.; Zhu, X.M.; Sun, D.; Wang, M. Investigation of interface compatibility during ball spinning of composite tube of copper and aluminum. *Int. J. Adv. Manuf. Technol.* **2017**, *88*, 683–690. [[CrossRef](#)]
23. Wang, T.; Gao, X.Y.; Zhang, Z.X.; Ren, Z.K.; Qi, Y.Y.; Zhao, J.W. Interfacial bonding mechanism of cu/al composite plate produced by corrugated cold roll bonding. *Rare Metals.* **2021**, *40*, 1284–1293. [[CrossRef](#)]

**Disclaimer/Publisher’s Note:** The statements, opinions and data contained in all publications are solely those of the individual author(s) and contributor(s) and not of MDPI and/or the editor(s). MDPI and/or the editor(s) disclaim responsibility for any injury to people or property resulting from any ideas, methods, instructions or products referred to in the content.